Kinetic Separation by Pressure Swing Adsorption: Method of Characteristics Model

A theoretical model using the method of characteristics is presented for a Skarstrom-type pressure swing adsorption (PSA) cycle using carbon molecular sieve for the kinetic separation of nitrogen/methane mixtures. Good agreement with experimental results was obtained. The solution of the reduced nonlinear ordinary differential equations along characteristics, a variable computational grid from the changing bed velocity, and a constant product flow boundary condition are complications that prohibited using the method of characteristics in favor of finite difference or orthogonal collocation methods. These complications have been overcome in the present study to develop a theoretical model, incorporating nonlinear isotherms and a linear driving force rate for diffusion, which requires less computer time and is particularly amenable for studying transient bed dynamics. The effects of feed pressure and concentration, half-cycle time, and product flow rate on kinetic PSA performance are also illustrated.

Mark W. Ackley
Ralph T. Yang
Department of Chemical Engineering
State University of New York
Buffalo, NY 14260

Introduction

Pressure swing adsorption (PSA) is an important process for separation of gas mixtures and has been commercialized for air drying, hydrogen purification, air separation, and various other separations (Yang, 1987). In the PSA process a high-pressure gas feed mixture is introduced to a column of packed sorbent where one or more components of the mixture are adsorbed, producing a purified stream of gas at the column exit, the sorbent bed is then regenerated by purging or evacuation at low pressure producing a countercurrent gas stream enriched in the sorbate at the column inlet, and the cycle is repeated indefinitely to separate the feed mixture into the desired enriched component streams. Most commercial PSA processes are of multibed design to generate a near-continuous product stream. Many variations of the simplified process described above have been introduced to improve overall process performance.

Separation of a gas mixture by PSA is generally accomplished by either selective adsorption (equilibrium separation) or by differences in component gas diffusion rates in the granular sorbent (kinetic separation). A third mechanism (steric separation) is inherent to zeolite materials and is the result of molecular sieving where one or more components of the mixture are excluded from entering the internal structure of the zeolite particle.

Models for equilibrium separation rely on the assumption of local equilbrium between the solid and gas phases in the packed bed. The method of characteristics has been applied extensively to reduce the partial differential equations (PDEs) to ordinary differential equations (ODEs) whereupon an analytic solution is obtained (Turnock and Kadlec, 1971; Shendalman and Mitchell, 1972; Mitchell and Shendalman, 1973; Chan et al., 1981; Knaebel and Hill, 1985). Kayser and Knaebel (1989) identify some of the major challenges remaining in modeling equilibrium PSA separations.

In the present study, the method of characteristics has been introduced to model the kinetic separation of binary gas mixtures in PSA processes. In contrast to equilibrium separation models, where a single characteristic represents the motion of a concentration wave front, a family of characteristics in the kinetic model represent the continuous development of the gas concentration profile in the bed. Incorporated in this model are the LDF (linear driving force) representation for mass transfer rates and the extended Langmuir equations for mixed gas isotherms. The model has been developed for a simple Skarstrom-type PSA cycle, with evacuation replacing the blowdown and purge steps.

The development of commercially viable alternative separation methods for upgrading natural gas depends upon achieving pipeline quality at lower costs than can currently be attained from cryogenic distillation. Separation of N_2/CH_4 mixtures on CMS represents one of the most challenging kinetic separation

problems due to the small difference in kinetic diameters of the gas molecules, the relatively low diffusivities of both gases, the modest kinetic separation factor, and the undesirable equilibrium selectivity toward methane. A single-bed PSA apparatus was constructed and operated to separate a 50/50 CH_4/N_2 mixture using Bergbau Forschung carbon molecular sieve (CMS). Pure gas adsorption isotherms and diffusion rates for this CMS were independently measured and used as physical data in the model. The model was used to study the bed dynamics in both the transient and cyclic steady-state regimes, as well as to predict overall process performance. Excellent agreement between model predictions and experimental results was obtained.

Adsorption and Diffusion Data for CMS

Carbon molecular sieve manufactured by Bergbau Forschung for PSA air separation (N_2 production) was used in this study. Pure gas equilibrium adsorption isotherms were measured at 295 K and are shown in Figure 1. The adsorption data for N_2 and CH_4 were fit to the Langmuir isotherm and the resulting constants (b_i, q_{mi}) are given in Table 1 ($i = 1$ for N_2, $i = 2$ for CH_4).

The rate of uptake of each gas was measured gravimetrically at 1.0 atm using both full-size pellets and crushed CMS. Since particle size had negligible effect upon the rate data, it was concluded that diffusion is micropore-controlled. Diffusion time constants were obtained by analyzing the data at short times (m_t/m_∞ vs. $\sqrt{t}$) and at long times (ln $[1-m_t/m_\infty]$ vs. t) as suggested by Ruthven et al., 1986). Values of D/r^2 obtained from a plot of ln $[1 - m_t/m_\infty]$ vs. t are given in Table 1 and are consistent with time constants obtained from the initial rate data. The kinetic separation factor (ratio of D/r^2 values) is 27. Although N_2 diffuses faster into the CMS, the isotherm data reveal a CH_4 equilibrium selectivity—a potentially adverse condition since CH_4 is the desired product. The adsorption and diffusion data obtained in this study compare favorably with independent measurements for CH_4 (Kapoor and Yang, 1989) and for N_2 (Ruthven et al., 1986) on a similar CMS.

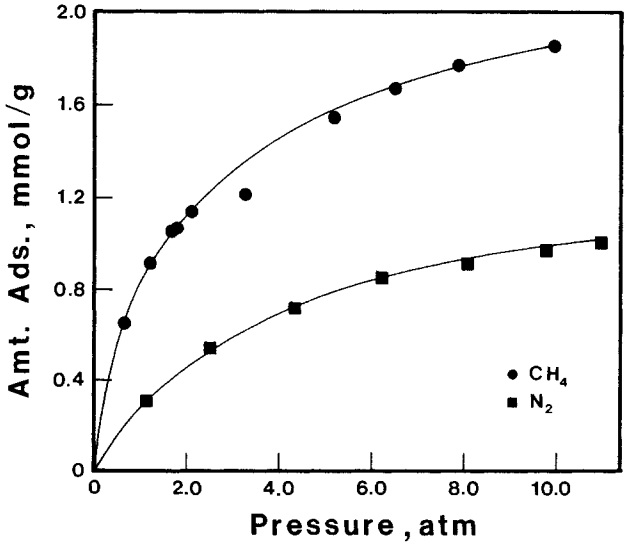

Figure 1. Equilibrium isotherms on Bergbau Forschung carbon molecular sieve at 295 K.

Table 1. Bed Parameters and Physical Characteristics of Carbon Molecular Sieve

Column Dimensions		
Diameter	4.1 cm	
Length	60.6 cm	
Cross-sectional area	13.2 cm^2	
Adsorbent	Bergbau-Forschung CMS	
Particle size	0.318 cm dia. pellets	
Bed void fraction	0.40	
Bulk density	0.708 g/cm^3	
Sorbent weight	566.4 g	
	N_2	CH_4
Langmuir Constants		
b_i atm^{-1}	0.2475	0.5882
q_{mi} mol/g	1.370×10^{-3}	2.125×10^{-3}
Diffusion Time Constant		
D/r^2 s^{-1}	9.3×10^{-5}	3.4×10^{-6}

PSA cycle

A simple Skarstrom PSA cycle was modified by replacing the blowdown and purge steps with a single evacuation step. The purge step is eliminated due to not only the slow diffusivity but strong adsorptive characteristics of CH_4 on this CMS. The evacuation step can be divided into a rapid depressurization step and a constant pressure desorption step. Since there is no purge, this system can be operated as a single-bed process as depicted in Figure 2. Also shown in this figure is an actual pressure/time history corresponding to this four-step process.

Assumptions imposed on this PSA process include:

- Rapid pressurization and depressurization

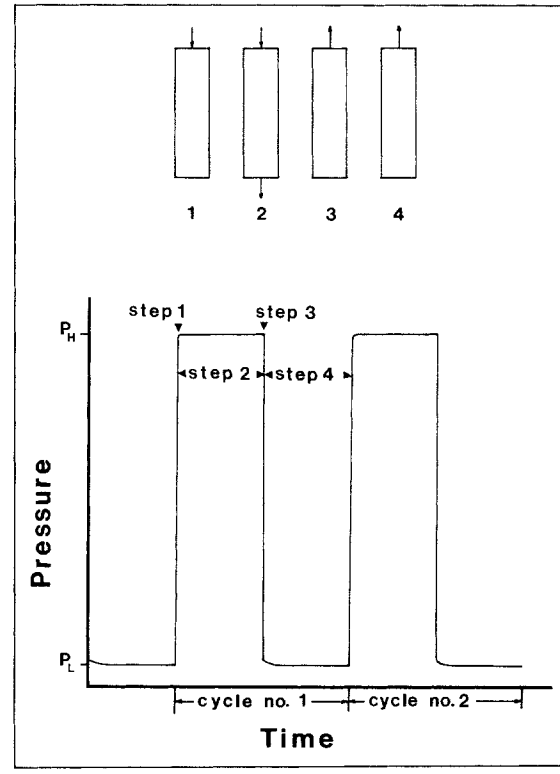

Figure 2. Four-step PSA cycle and pressure history.

- Constant pressure feed and evacuation
- Frozen solid phase during pressure changing steps
- Uniform gas-phase concentration throughout the bed at the feed composition at the end of the pressurization step.

The four-step cycle can now be approximated mathematically as a two-step cycle, i.e., adsorption-desorption.

The above PSA cycle is to be operated at a constant product flow rate. This facilitates the experiments but complicates the solution of the model equations. The implications of constant product flow rate upon the solution of the differential equations is discussed later in this paper. The overall material balance (for the feed step) dictates that only one of the two flow rates (feed or product) may be controlled while maintaining a constant bed pressure.

Experimental Apparatus

A single-bed PSA apparatus was constructed to produce the cycle steps illustrated in Figure 2. A schematic of the apparatus is shown in Figure 3. Bed parameters are summarized in Table 1.

A high-pressure gas mixture containing 50% each of CH_4 and N_2 was introduced to the column during steps 1 and 2. Product was withdrawn at a constant rate during step 2. Steps 3 and 4 were combined as one step in the experiments by evacuating the bed countercurrently. Bed pressure was controlled in step 2 by a pressure regulator. A programmed timer controlled solenoid valves to achieve the desired cyclic operation. Product purity was determined by withdrawing gas samples from the product stream and analyzing in a gas chromatograph equipped with a thermal conductivity detector (TCD). Total volumes of product and gas desorbed during evacuation were measured using a wet test meter.

Prior to each PSA experiment, the bed was regenerated at 360 K in He flow for approximately 24 hours, allowed to cool to room temperature, and then evacuated to P_L. A thermocouple inserted in the bed was used to monitor cyclic temperature variations.

Approximately 10–15 cycles were required to reach cyclic steady state. All PSA experiments were carried out for 20 cycles. The maximum temperature swing measured in any PSA cycle was 4.8°C.

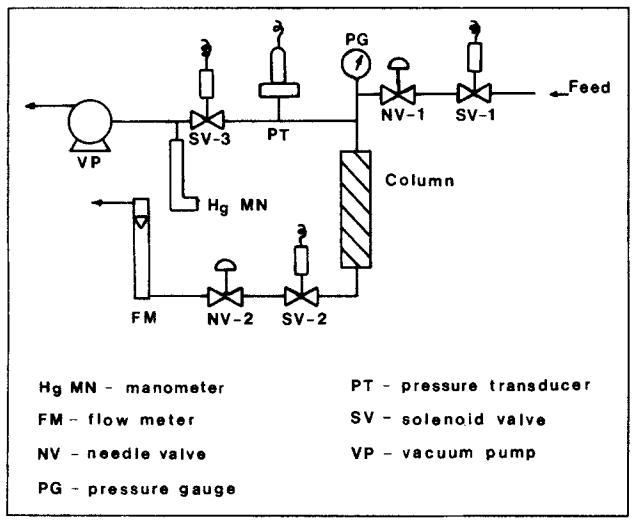

Figure 3. PSA aparatus.

Mathematical Model

The material balance for each component in the bed can be represented as follows:

$$\frac{\partial C_i}{\partial t} + \frac{\partial (uC_i)}{\partial z} + \left[\frac{1-\epsilon}{\epsilon}\right]\frac{\partial \bar{q}_i}{\partial t} = 0 \tag{1}$$

Assumptions implicit in Eq. 1 are: negligible axial dispersion, isothermal bed, and axisymmetric plug flow.

Finite mass transfer resistances have been approximated by a linear driving force (LDF):

$$\frac{\partial \bar{q}_i}{\partial t} = k_i(q_i^* - \bar{q}_i) \tag{2}$$

where $k_i = \Omega_i (D/r^2)_i$, and $\Omega_i = f(\theta_{ci})$. Amounts of each gas adsorbed from the binary mixture at equilibrium (q_i^*) are approximated using the extended Langmuir isotherm:

$$q_i^* = \left(\frac{\rho_B}{1-\epsilon}\right)\frac{q_{mi} b_i y_i P}{1 + b_1 y_1 P + b_2 y_2 P} \tag{3}$$

The diffusion time constants $(D/r^2)_i$ are those determined from the pure gas uptake measurements. When the dimensionless cycle time $\theta_c > 0.1$, the Glueckauf approximation ($\Omega_i = 15$) is reasonable (Yang, 1987). For small values of θ_c, however, it has been shown that $\Omega_i = 15$ underpredicts the rate of uptake (Nakao and Suzuki, 1983; Raghavan et al., 1986). A variation of Ω_i with θ_c was developed in those studies to compensate for the inadequacy of the Glueckauf constant under cyclic conditions when the total amount adsorbed is small. The effect of Ω_i has been investigated in the present model.

A mass balance for each component can be written in terms of (y_i, P, u) by applying the ideal gas law. The overall mass balance is then obtained by adding the two transformed component equations. Combining the transformed equations for the overall and component 2 mass balances produces:

$$\frac{\partial y_2}{\partial t} + u\frac{\partial y_2}{\partial z} = \frac{RT}{P}\left[\frac{1-\epsilon}{\epsilon}\right]\left[(y_2 - 1)\frac{\partial \bar{q}_2}{\partial t} + y_2\frac{\partial \bar{q}_1}{\partial t}\right] \tag{4}$$

Since the bed pressure is constant during the adsorption and desorption steps ($\partial P/\partial t = 0$) and the pressure drop can be considered negligible ($\partial P/\partial z \simeq 0$), the overall mass balance can be further simplified:

$$\frac{\partial u}{\partial z} = -\frac{RT}{P}\left[\frac{1-\epsilon}{\epsilon}\right]\left[\frac{\partial \bar{q}_1}{\partial t} + \frac{\partial \bar{q}_2}{\partial t}\right] \tag{5}$$

Equations 2, 4 and 5 form the set of governing PDEs. It is not necessary to solve this set of equations during the pressure changing steps due to the frozen, solid-phase approximation.

Similar sets of quasilinear PDEs have previously been formulated to represent kinetic separation in PSA processes. Whereas these other studies have utilized either finite difference (Kapoor and Yang, 1989; Doong and Yang, 1986) or orthogonal collocation (Farooq and Ruthven, 1990; Raghavan and Ruthven, 1985; Hassan et al., 1987; Shin and Knaebel, 1987) solution methods, the present work introduces the method of characteristics in its entirety for modeling kinetic separation.

Solution by Method of Characteristics

Characteristics may be viewed in the Lagrangian sense as the trajectories of gas molecules as they move through the bed. These trajectories are also the paths along which disturbances at the inlet or at boundaries propagate. When two characteristics of the same family intersect, a shock discontinuity arises. The use of the method of characteristics in PSA equilibrium separation exploits this condition. Parallel or divergent characteristics constitute a family of simple waves with no shocks. These two distinct types of waves fundamentally distinguish equilibrium from diffusion-controlled adsorption.

A sharp wave front is indicative of a narrow mass transfer zone that moves through the bed in equilibrium adsorption processes. The motion of this wave front or shock is described by a single characteristic. The accompanying ODE is solved for the pressure changing steps to determine gas composition behind the wave front (Chan et al., 1981). Analytic solutions have been obtained using this method for purification and air-drying PSA processes when the governing ODEs are linear, including linear isotherms.

Conversely, kinetic separation is characterized by finite mass transfer rates that cause the mass transfer zone to envelope the entire bed. Simple waves dominate these processes because of the strong dissipative effects of finite mass transfer resistances. Shock waves, however, can occur during the initial phases of any PSA step and become a major complication in nonlinear systems because their location is not known *a priori*. Shock discontinuities are avoided and characteristics are maintained as simple waves in the inherently nonlinear kinetic separation by ensuring continuous initial and boundary conditions. A more complete discussion of this method is given elsewhere (Aris and Amundson, 1973).

Reduction of PDEs to ODEs

In applying the method of characteristics, a direction is found in the solution surface along which the total derivative of the dependent variable may be represented, allowing the PDE to be reduced to an ODE. The characteristics in the solution surfaces are projected into the (z,t) plane, and the system of ODEs are then solved along these characteristics using standard numerical methods.

For example, the lefthand side of Eq. 4 can be represented as the total derivative of $y_2(z,t)$ along the characteristic direction defined by:

$$\frac{dt}{dz} = \frac{1}{u} \tag{6}$$

Equations 2 and 5 are similarly reduced to ODEs that must be solved along their corresponding characteristics. The ODEs were further simplified by introducing the dimensionless variables, $\xi = z/L$, $\tau = t/t_c$, and $\omega = u/u_1$. The set of four ODEs and the corresponding characteristics are given in final form in Table 2.

The reference velocity (u_1) is the inlet feed velocity at the start of the first cycle (clean bed). Applying an overall mass flow rate balance at $\tau = 0$ to determine the incipient flow rate gives u_1:

$$u_1 = \left[\frac{RT}{P\epsilon A_c}\right]\left[\frac{(1-\epsilon)W_s}{\rho_B}(k_1 q_1^* + k_2 q_2^*) + \dot{m}_p\right] \tag{7}$$

Table 2. Governing Set of Dimensionless ODEs

Dimensionless Ordinary Differential Eqs. to be Solved along "Characteristics"	"Characteristic" Eqs. in ξ-τ Plane	
$\left(\frac{dy_2}{d\tau}\right)_{\mathrm{I}} = A\left[(y_2 - 1)\frac{d\bar{q}_2}{d\tau} + y_2\frac{d\bar{q}_1}{d\tau}\right]$	$\frac{d\tau}{d\xi} = \frac{B}{\omega}$	(I)
$\left(\frac{d\omega}{d\xi}\right)_{\mathrm{II}} = -AB\left[\frac{d\bar{q}_1}{d\tau} + \frac{d\bar{q}_2}{d\tau}\right]$	$\tau = \text{const.}$	(II)
$\left(\frac{d\bar{q}_i}{d\tau}\right)_{\mathrm{III}} = k_i t_c(q_i^* - \bar{q}_i)$	$\xi = \text{const.}$	(III)
$A = \frac{RT}{P}\left[\frac{1-\epsilon}{\epsilon}\right]$	$B = \left[\frac{L}{u_1 t_c}\right]$	

Initial and boundary conditions

The equations in Table 2 are generally applicable to fixed bed adsorption. However, the initial and boundary conditions are derived from the PSA cycle conditions. The idealized two-step process is started with a clean bed at the adsorption step.

Initial Conditions:

$$\tau = 0, \quad y_2 = y_{2f}, \quad \omega = 1.0, \quad P = P_H$$

Boundary Conditions:

Adsorption step:

$$\begin{aligned} \omega &= \omega_P \quad \text{at} \quad \xi = 1.0 \\ y_2 &= Y_{2f} \quad \text{at} \quad \xi = 0.0 \\ P &= P_H \quad \text{at} \quad 0.0 \le \xi \le 1.0 \end{aligned}$$

Desorption step:

$$\begin{aligned} \omega &= 0 \quad \text{at} \quad \xi = 1.0 \\ \frac{dy_2}{d\xi} &\simeq 0 \quad \text{at} \quad \xi = 1.0 \\ P &= P_L \quad \text{at} \quad 0.0 \le \xi \le 1.0 \end{aligned}$$

The solid-phase concentration distributions $q_1(\xi)$ and $q_2(\xi)$ at the end of each step become the initial distributions in the bed for the following step. The gas-phase concentration is assumed to be uniform throughout the bed at the feed concentration at the beginning of each adsorption step—a reasonable condition when the pressure is low prior to the pressurization step and when the frozen-bed approximation is valid. This condition avoids the formation of a shock discontinuity in the adsorption step. The gas-phase concentration distribution $y_2(\xi)$ at the end of the adsorption step is used as the initial distribution at the beginning of the desorption step, but at the desorption pressure P_L.

Solution technique

The application of the method of characteristics to noncyclic, one-dimensional heat and mass transfer in packed beds has been summarized by Acrivos for initial-value problems, in which the rate of flow and the composition of the entering feed are known

functions of time (Acrivos, 1956). The solution strategy must be altered for the cyclic PSA process since inlet (feed) velocity is unknown. In the adsorption step, an inlet velocity is estimated and the equation set is solved along a family II characteristic to give the solid-phase concentration distributions $q_1(\xi)$ and $q_2(\xi)$. The total amount of gas adsorbed through time τ_{n+1} can then be determined:

$$Q_{n+1} = \frac{(1-\epsilon)W_s}{\rho_B}\int_0^1 (\bar{q}_1(\xi) + \bar{q}_2(\xi))_{n+1} d\xi \qquad (8)$$

An average inlet velocity is then computed from a mass flow rate balance:

$$\bar{u}_f = \left[\frac{RT}{P}\right]\left[\frac{1}{\epsilon A_c}\right]\left(\frac{\Delta Q_n}{\Delta\tau t_c} + \dot{m}_P\right) \qquad (9)$$

where ΔQ_n represents the incremental amount adsorbed during the time interval τ_n to τ_{n+1}. The average inlet velocity ($\bar{u}_f$) over this time interval is then used to improve the estimate of inlet velocity (u_f) at τ_{n+1}, and the entire process is repeated along τ_{n+1} until consecutive calculations of u_f converge. Iteration on velocity is not required in the desorption step since the velocity at the closed end of the bed is zero. However, an initial step size ($\Delta\xi_P$) must be selected in this step since the characteristic equation gives an infinite slope for $d\tau/d\xi$ for $\omega = 0$.

The modified Euler method was selected because of its adaptability to variable step sizes, the minimal number of functional evaluations required, and fast convergence. The characteristic equation $d\tau/d\xi = B/\omega$ determines the slope of family I characteristics and establishes the relationship between the dimensionless time and distance step sizes. Since the time step size ($\Delta\tau$) is fixed in this model, the distance ($\Delta\xi$) varies according to the characteristic equation—such variation tied to the change in velocity (ω) throughout the bed.

The locations of the computational grid points along each family II characteristic are not known at the beginning of the solution process and must be determined iteratively. The characteristic equation defining $\Delta\xi_{m+1}$ is linked through the velocity to the ODE equation set and thus is coupled to all of the dependent variables. As a result, the grid points were established in this model based on the convergence of the distance stepsize $\Delta\xi_{m+1}$ alone.

The position of grid points at successive times (τ_{n+1}) are not necessarily collinear in ξ since velocity ω varies with time as well as with bed position. This introduces a complication in that values of the dependent variables determined in the previous computation along τ_n are required in the solution along τ_{n+1}. This problem was overcome by fitting $q_1(\xi)$, $q_2(\xi)$, and $y_2(\xi)$ continuously over $0 \le \xi \le 1$ using a cubic spline. The cubic spline also provides a convenient means of integrating $q_1(\xi)$ and $q_2(\xi)$ as required in Eq. 8.

Using the solution methods described above, a computer model was developed and applied to investigate a wide range of conditions for the CH_4/N_2/CMS PSA process. The typical CPU time for a 25-cycle run on a VAX 8800 is approximately 7.5 min or 18 s/cycle. This compares approximately to a CPU time of 100 s/cycle for a similar PSA problem solved by finite difference methods on the same type of computer (Kapoor and Yang, 1989). Convergence in the method of characteristics is inherent and fast, and the technique allows easy extraction of dependent variable distributions in both time and bed position.

Discussion of Results

Predictions using the mathematical model were compared to measurements of actual PSA performance. Product purity and recovery, feed rate, and throughput at cyclic steady state and the transient behavior of the average product purity were used to determine the effectiveness of the model. Recovery is defined as:

$$\%\ \text{Recovery}\ CH_4 = \frac{n_P\bar{y}_2}{n_f y_{2f}} \times 100 \qquad (10)$$

where $\bar{y}_2$ represents the average product purity over the adsorption half-cycle. Throughput is computed:

$$\text{Throughput [L(STP)/h/kg]} = \frac{1{,}000\ V_f}{2t_c W_s} \qquad (11)$$

PSA experiments were performed over the following ranges of conditions: 2.0 atm $\le P_H \le$ 6.0 atm, 600 s $\le t_c \le$ 1,800 s, and 50 cm^3/min $\le Q_P \le$ 400 cm^3/min. Results of PSA experiments are summarized along with the corresponding model predictions in Table 3.

Effect of Ω_i

The effect of Ω_2 on model predictions was investigated by selecting Ω_2 values of 15, 30 and 40 while maintaining $\Omega_1 = 15$. PSA conditions were chosen identical to those for experiment no. 10. The variation of product purity throughout the feed cycle at cyclic steady state is illustrated in Figure 4a, while the approach to cyclic steady state is shown in Figure 4b. $\Omega_2 = 15$ gives the best agreement with the experimental results.

The cyclic parameter Ω_i was introduced by Nakao and Suzuki to correct inadequacies of the LDF model by considering single-particle pore diffusion (Nakao and Suzuki, 1983). Raghavan et al. extended this reasoning to packed beds and established $\Omega = 15$ for $\theta_c \ge 0.1$, $\Omega = 40$ for $\theta_c \le 0.01$, for micropore-controlled diffusion for a four-step PSA cycle (Raghavan et al., 1986). Kapoor and Yang applied these concepts to determine empirically a set of Ω_i coefficients in the separation of CO_2/CH_4 on CMS (Kapoor and Yang, 1989).

In the present study, θ_c for N_2 varies from 0.056 at $t_c = 600$ s to 0.17 for $t_c = 1{,}800$ s, while $\theta_c = 2.0 \times 10^{-3}$ at $t_c = 600$ s and $\theta_c = 6.1 \times 10^{-3}$ at $t_c = 1{,}800$ s for CH_4. Thus, $\Omega_1 = 15$ is reasonable for nitrogen diffusion in this CMS. The lower values of θ_c for CH_4 suggest $\Omega_2 = 40$ if the findings of Raghavan et al. (1986) are followed.

When values of Ω_i are empirically determined to achieve the best fit with experimental data, one attempts to correct all of the inadequacies of the model (not just those due to the LDF approximation) in the parameters Ω_i. The extended Langmuir binary isotherms and the use of pure gas diffusion time constants $(D/r^2)_i$ in the model are approximate representations of the true physical phenomena that potentially introduce inaccuracies at least as great as those from the LDF approximation. The results of Raghavan et al. were obtained for a dilute single-adsorptive (Raghavan et al., 1986) and do not reflect the potential effects of mixture thermodynamics, mixture diffusion rates, and velocity change in the bed. For these reasons, the simple Glueckauf

Table 3. Summary of PSA Experiments and Model Predictions

Exp. No.	P_H atm	P_L atm	t_c s	Q_P cm³/min	CH_4 Purity %	Feed Rate mol/Cycle	CH_4 Recovery %	Throughput L STP/h/kg
14	3.97	0.030	900	49.4	75.7	0.208	22.4	17.7
Model					74.7	0.163	28.3	13.9
8	3.99	0.030	900	200	74.2	0.325	56.5	27.7
Model					66.6	0.270	61.5	23.1
9	3.98	0.034	900	397	66.3	0.458	71.4	39.0
Model					60.2	0.398	75.0	34.0
13	3.97	0.034	600	47.5	72.9	0.175	16.4	22.4
Model					69.8	0.136	20.4	17.4
10	2.01	0.026	900	52.5	77.8	0.139	36.9	11.9
Model					77.6	0.116	43.9	9.9
11	2.00	0.023	1,800	48.9	79.2	0.198	48.5	8.5
Model					80.2	0.178	55.0	7.6
12	5.97	0.038	900	49.3	72.6	0.253	17.6	21.6
Model					70.9	0.207	21.1	17.7

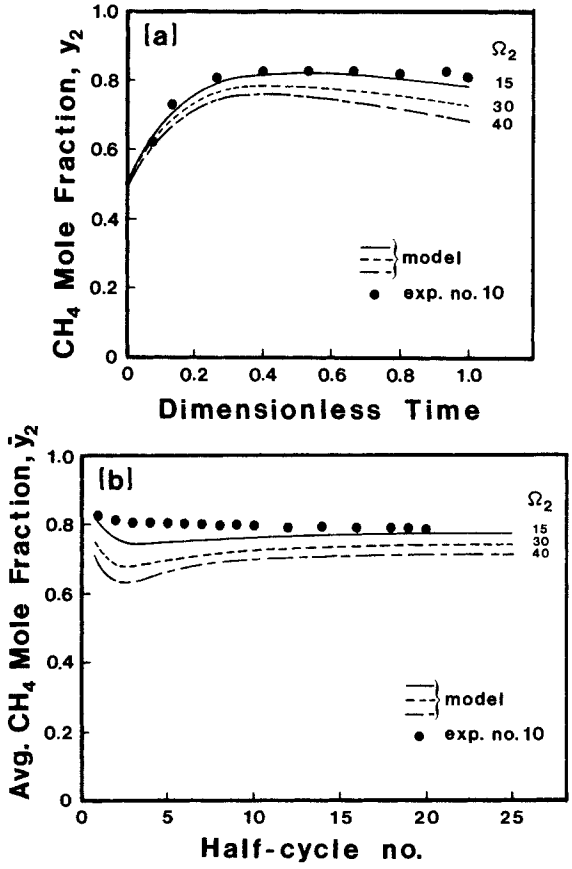

Figure 4. Effect of the LDF parameter (Ω_2) on product purity.

a) At cyclic steady state
b) In approach to cyclic steady state
Data from experiment no. 10.
PSA conditions: $P_H = 2.01$ atm, $P_L = 0.026$ atm, $t_c = 900$ s, $Q_P = 52.5$ cm³/min

approximation ($\Omega_i = 15$) was retained for both N_2 and CH_4 throughout this study.

Bed dynamics

The behavior of the inlet velocity and parameter distributions within the bed have been demonstrated from model calculations using a single set of PSA conditions: $P_H = 4.0$ atm, $P_L = 0.02$ atm, $t_c = 900$ s, and $Q_p = 50$ cm³/min. Conservation of mass dictates a self-adjusting feed rate when the bed pressure and product flow rate are controlled at constant values during the adsorption step. Dimensionless inlet velocity (and thus feed rate) variation is shown in Figure 5. Inlet velocity decreases by more than a factor of two during the course of any given adsorption half-cycle and would eventually approach the con-

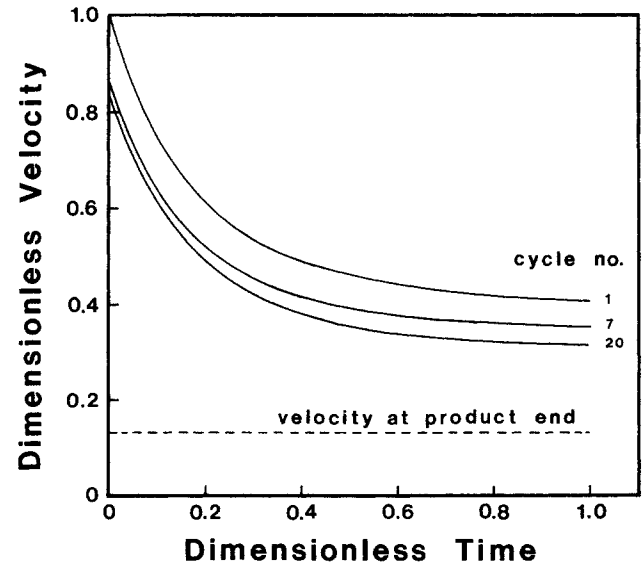

Figure 5. Inlet (feed) velocity variation with dimensionless time and cycle no.

PSA conditions: $P_H = 4.0$ atm, $P_L = 0.02$ atm, $t_c = 900$ s, $Q_P = 50$ cm³/min

stant product velocity in the limit if the bed were allowed to saturate, i.e., when adsorption ceases. The approach to the cyclic steady state is also shown in Figure 5.

The gas-phase concentration of CH_4 at the end of the adsorption cycle increases over the entire bed length as shown in Figure 6a. Similarly, the dimensionless velocity distribution in the bed at cyclic steady state is illustrated in Figure 6b. The velocity decreases continuously through the bed as gas diffuses into the CMS.

The amounts of each gas exchanged during the adsorption and desorption steps of the PSA cycle are determined from the areas between the solid-phase concentration profiles at the end of these steps as shown in Figure 7. The greater selectivity of methane by this CMS results in CH_4 solid-phase concentrations much higher than those of N_2. However, separation is determined by the relative amounts of the gases adsorbed in the feed step (or desorbed in the evacuation step), and it is evident from Figure 7 that considerably more N_2 is exchanged than CH_4.

The solid-phase concentration profiles at the end of the adsorption step (Figure 7) are similar in character to the respective gas-phase distributions shown in Figure 6a. More N_2 is exchanged at the feed end of the bed than at the product end, while the reverse is true for CH_4. The nature of the CH_4 (strong

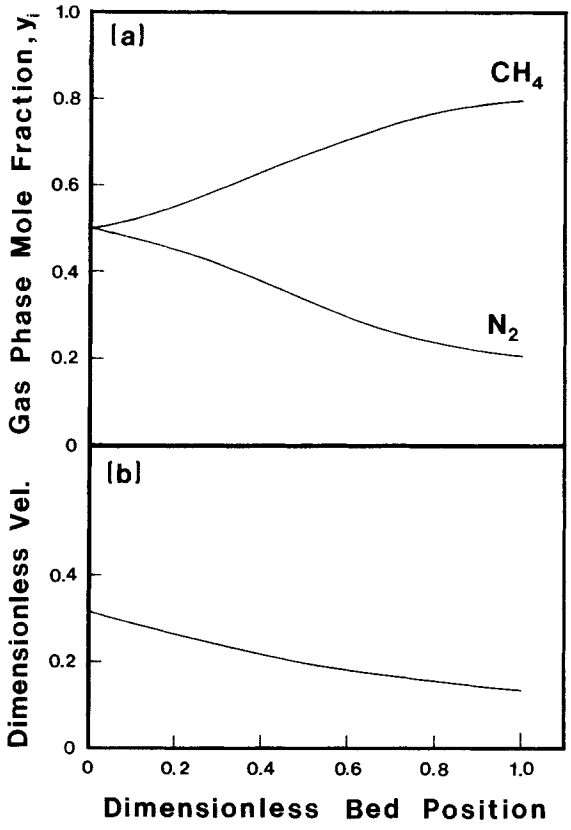

Figure 6. Gas-phase concentration and velocity distributions at the end of the adsorption step as a function of dimensionless bed position at cyclic steady state.

a) Gas-phase concentration of CH_4 and N_2 within the bed
b) Interstitial bed velocity variation
PSA conditions: $P_H = 4.0$ atm, $P_L = 0.02$ atm, $t_c = 900$ s, $Q_P = 50$ cm^3/min

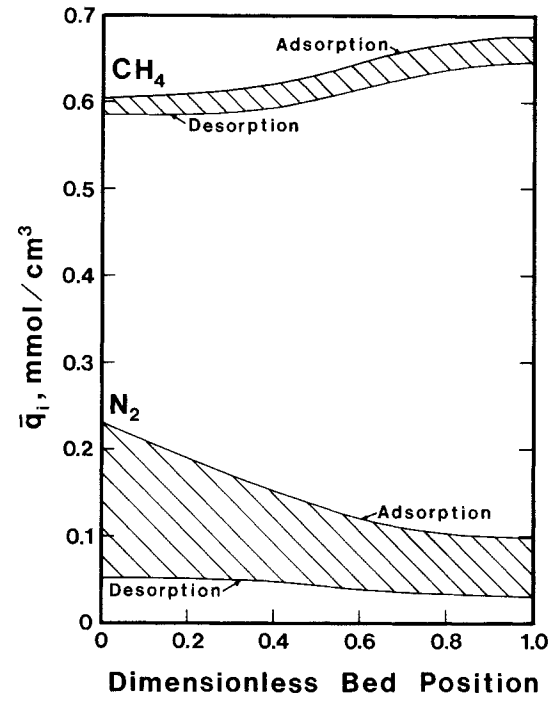

Figure 7. Solid-phase concentration profiles at the end of adsorption and desorption steps as a function of dimensionless bed position at cyclic steady state.

PSA conditions: $P_H = 4.0$ atm, $P_L = 0.02$ atm, $t_c = 900$ s, $Q_P = 50$ cm^3/min

adsorptive but slow diffusing component) solid-phase distributions contrasts that of N_2 and can be explained by considering Eqs. 2 and 3 with Figures 6a and 7. The value of the solid-phase concentration $\bar{q}_2$ in the LDF equation can be found in the shaded area between the adsorption/desorption boundary curves in Figure 7 for any position in the bed (ξ = constant). The second driving force term (q_i^*) is determined from Eq. 3. During the high-pressure feed step q_i^* is dependent solely on y_i. Since y_2 increases much more near the product end than at the feed end (over the course of the adsorption step) relative to the corresponding change in $\bar{q}_2$, the average value ($q_2^* - \bar{q}_2$) is higher at the product end. It can also be argued that qi^* is small compared to $\bar{q}_i$ for all y_i during the desorption step because of the dominance of the low value of P_L in Eq. 3. Thus, the average desorption rate is dominated by $\bar{q}_i$ in Eq. 2.

Solid-phase concentrations resulting from kinetic separation in PSA processes have not been widely discussed in the literature, except for those limited to the fast diffusing component (Raghavan and Ruthven, 1985). Although the higher overall solid-phase concentration of the product shown in this study is somewhat unusual due to the higher selectivity of CH_4 on the CMS, the overall character of the distributions in Figure 7 is believed to be representative of more general, kinetically-controlled PSA separations.

The accumulation of methane in the solid phase is illustrated in Figure 8 where solid-phase concentration averaged over the entire bed $\overline{\bar{q}_2}$ at the end of the desorption cycle increases through the first 40 cycles, while the average nitrogen concentration changes very little beyond 20 cycles. However, the actual

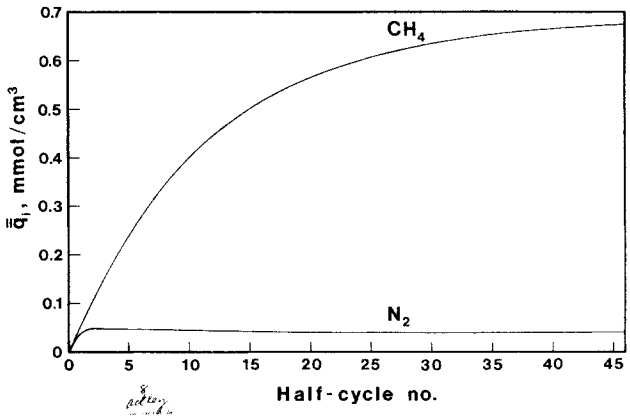

Figure 8. Accumulation of gases in solid phase in approach to cyclic steady state.

Average solid-phase concentration at the end of the desorption step as a function of half-cycle no.
PSA conditions: $P_H = 4.0$ atm, $P_L = 0.02$ atm, $t_c = 900$ s, $Q_P = 50$ cm^3/min

separation of the two gases is not greatly effected after 20 cycles: the product purity for the PSA cycle of Figure 9 increases only from 74.6% in cycle no. 20 to 75.1% in cycle no. 50.

PSA performance

CH_4 purity in the product is measured directly throughout the feed half-cycle and thereby serves as a good indicator of model effectiveness. The y_2 values from model and experiment compare well in most cases as shown by the results in Figures 4 and 9a. The greatest difference between prediction and measurement of y_2 occurs at high product flow rates where $Q_P = 200$, 400 cm^3/min. Although the model underpredicts product purity at these higher flow rates as shown in Figure 9b, the variation of y_2 throughout the cycle is closely matched.

The effective separation factor decreases with increasing Ω_2 as demonstrated by the results in Figure 4. It appears from Figure 9b that the separation factor in the model is appropriate, but that the overall mass transfer rates for both gases should be proportionately higher. Since mass transfer limitations from the bulk flow have been ignored in the model, a possible reason for the higher measured purity at higher product flow rates is that the mass transfer resistance for diffusion from the bulk flow is reduced at the higher bed velocities.

The average purity of CH_4 ($\bar{y}_2$) decreases with increasing product flow rate, as illustrated in Figure 10 where feed and evacuation pressures have been held constant at 4.0 atm and 0.02 atm, respectively. Maximum purity is achieved at product flow rates less than 50 cm^3/min, increasing with increasing values of t_c. The influence of product flow rate on product purity for $Q_P > 50$ cm^3/min becomes stronger with increasing half-cycle time. In the range $Q_P > 200$ cm^3/min, the average purity increases with decreasing t_c for $900\ s \le t_c \le 2{,}400$s, $\bar{y}_2$ decreasing again for $t_c = 600$ s. These results demonstrate the complex coupling of the dependent variables: performance trends may be entirely reversed in different ranges of the process conditions.

The best recovery of product is achieved at the highest product flow rates and longest half-cycle times. The purity, however, is lowest at these conditions. Conversely, the highest levels of CH_4 purity correspond to very low recovery values. The

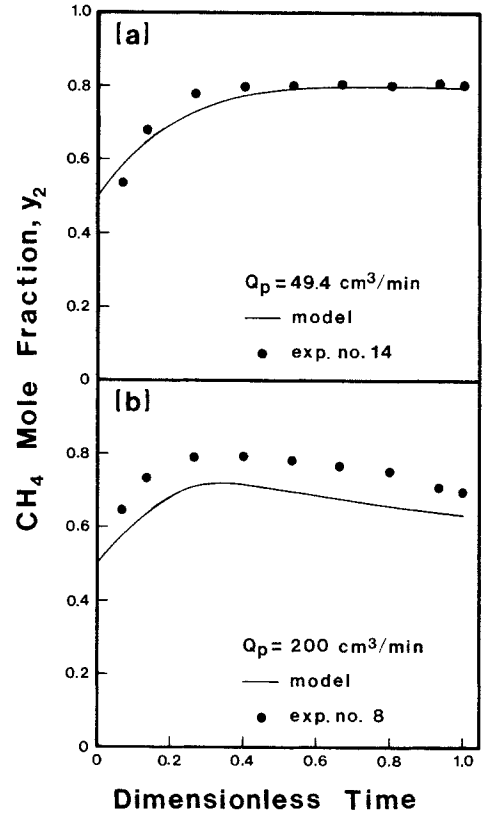

Figure 9. Effect of product flow rate on agreement between model and experimental results.

a) Product purity at cyclic steady state as a function of dimensionless time (exp. no. 14) for $P_H = 3.97$ atm, $P_L = 0.03$ atm, $t_c = 900$ s, $Q_P = 49.4$ cm^3/min
b) Product purity at cyclic steady state as a function of dimensionless time (exp. no. 8) for $P_H = 3.99$ atm, $P_L = 0.03$ atm, $t_c = 900$ s, $Q_P = 200$ cm^3/min
Solid lines represent model calculations.

results in Figure 10 suggest that overall PSA performance can be optimized in the range 50 cm^3/min $< Q_p <$ 100 cm^3/min for $t_c \ge 1{,}800$ s.

PSA performance is influenced by feed pressure as shown in Figure 11 for a constant product flow rate, $Q_P = 50$ cm^3/min. There appears to be an optimum pressure for maximizing product purity having such optimum increasing with increasing t_c. Recovery of product decreases with increasing feed pressure and is lowest at the shortest cycle times. The decrease in both product purity and recovery at the higher pressures is the result of the increasing mass of gas in the interparticle void space relative to that exchanged in each cycle step.

Measured PSA performance is compared with model predictions in Figure 11. Product purity results agree favorably with previous predictions. Although the effects of feed pressure and cycle time on recovery are correctly predicted by the model, recovery is consistently overpredicted. Because of the good agreement between model and experiment for product purity, the disagreements in recovery are likely due to measurement and/or prediction of the feed quantity. System dead volumes, small leaks, and any gas introduced by the exhaust of the vacuum pump in the evacuation cycle contribute to an inflated feed. The isotherm and pure gas diffusion rate input data to the model, the choice of the coefficients Ω_i, the estimation of the

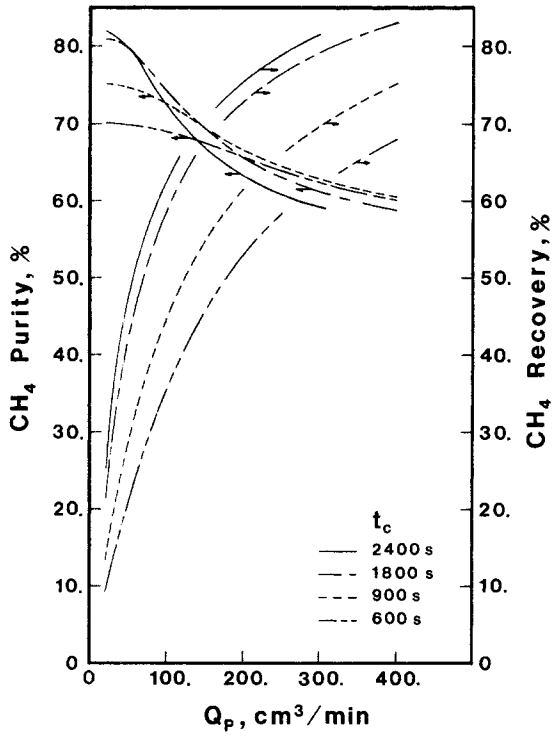

Figure 10. Effects of product flow rate and half-cycle time (t_c) on PSA performance at cyclic steady state.

Pressures constant at $P_H = 4.0$ atm and $P_L = 0.02$ atm

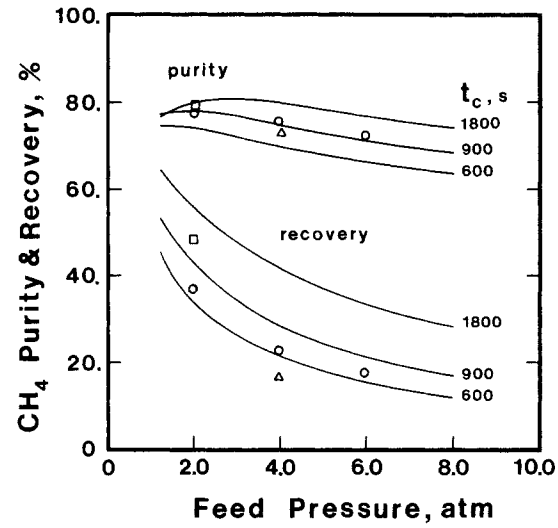

Figure 11. Effect of feed pressure and half-cycle time on PSA performance at cyclic steady state.

Product flow rate constant at $Q_P = 50$ cm³/min and desorption pressure contant at $P_L = 0.02$ atm

Experimental data given by symbols: □ $t_c = 1{,}800$ s, ○ $t_c = 900$ s, △ $t_c = 600$ s

Solid lines represent model calculations.

amount of gas introduced during the rapid pressurization step are all factors that can introduce errors to the feed rate prediction.

A methane product should be approximately 90% pure to be of commercial interest. Based on the performance profile provided in Figures 10 and 11, it is unlikely that 90% CH_4 purity is attainable using the simple PSA cycle of this study for a 50/50 feed mixture. Higher product purities are possible, however, for feed mixtures containing more than 50% CH_4. The model was used to study the effect of varying feed concentration, showing that 90% CH_4 purity can be achieved for feed mixtures containing 70% or more methane.

Conclusions

The method of characteristics provides an alternative approach to model kinetic separation of gas mixtures in PSA processes. The model consumes minimal computer time and can be conveniently applied to investigate prospective sorbents for a particular gas separation over a wide range of operating conditions. Independently measured pure-gas isotherms and diffusivities are the only physical data required in the model. The use of the Glueckauf coefficients in the LDF approximation results in reasonably good estimates of PSA performance without the aid of PSA experiments.

Acknowledgment

The authors are grateful to Drs. William J. Rae and John A. Tsamopoulos for their helpful discussions concerning the mathematical model and to M.S.A. Baksh for performing the gravimetric uptake measurements. This work was partially supported by NSF Grant CTS 8914754.

Notation

A_c = cross-sectional area of bed, cm²
b_i = Langmuir constant, atm^{-1}
C_i = component gas phase concentration, mol/cm³
$(D/r^2)_i$ = diffusion time constant, s^{-1}
k_i = mass transfer coefficient, s^{-1}
L = bed length, cm
$\dot{m}_P$ = product mass flow rate, mol/s
m_t = amount adsorbed at time t, g
n_f, n_P = total no. of moles of feed or product per cycle, mol
P = total gas phase pressure, atm
P_H, P_L = pressure during desorption or evacuation step, atm
$\bar{q}_i$ = component solid phase concentration, mol/cm³ solid
$\bar{\bar{q}}_i$ = $\bar{q}_i$ averaged over entire bed, mol/cm³ solid
q_i^* = component solid phase concentration in equilibrium with gas phase concentration C_i, mol/cm³ solid
q_{mi} = amount adsorbed for monolayer coverage, mol/g
Q_{n+1} = total gas adsorbed over time interval $0 \le \tau \le \tau_{n+1}$, mol
Q_P = product volume flow rate at STP, cm³/min
r = radius of carbon molecular sieve crystals, cm
R = gas constant = 82.0567 cm³ · atm · mol^{-1} K^{-1}
T = gas-phase temperature, K
t = time, s
t_c = half-cycle time, s
u = interstitial flow velocity, cm/s
u_1 = interstitial flow velocity at bed inlet at $t = 0$, cm/s
V_f = total volume (STP) of feed per cycle, L
W_s = weight of sorbent in bed, g
y_i = component mole fraction
z = distance along bed, cm

Greek letters

ρ_B = packed bed bulk density, g/cm³
ϵ = interpellet void fraction
$\xi = z/L$, dimensionless bed position
$\tau = t/t_c$, dimensionless time
$\omega = u/u_1$, dimensionless velocity

$\theta_c = Dt_c/r^2$, dimensionless cycle time
Ω_i = constant in LDF Eq. 3

Subscripts

i = component, $N_2 = 1$, $CH_4 = 2$
f = feed end of bed
p = product end of bed
∞, * = equilibrium

Literature Cited

Acrivos, A., "Method of Characteristics Technique, Application to Heat and Mass Transfer Problems," *Ind. Eng. Chem. Eng. Des. Proc. Dev.*, **48,** 703 (1956).

Aris, R., and N. R. Amundson, *Mathematical Methods in Chemical Engineering, Vol. 2, First-Order Partial Differential Equations with Applications,* Prentice-Hall, Englewood Cliffs, NJ (1973).

Chan, Y. N., F. B. Hill, and Y. W. Wong, "Equilibrium Theory of a Pressure Swing Adsorption Process," *Chem. Eng. Sci.*, **36,** 243 (1981).

Doong, S.-J., and R. T. Yang, "Bulk Separation of Multicomponent Gas Mixtures by Pressure Swing Adsorption: Pore/Surface Diffusion and Equilibrium Models," *AIChE J.*, **32,** 397 (1986).

Farooq, S., and D. M. Ruthven, "A Comparison of LDF and Pore Diffusion Models for a PSA Bulk Separation Process," *Chem. Eng. Sci.*, **45,** 107 (1990).

Hassan, M. M., N. S. Raghavan, and D. M. Ruthven, "Pressure Swing Air Separation on a Carbon Molecular Sieve: II. Investigation of a Modified Cycle with Pressure Equalization and No Purge," *Chem. Eng. Sci.*, **42,** 2037 (1987).

Kapoor, A., and R. T. Yang, "Kinetic Separation of Methane-Carbon Dioxide Mixture by Adsorption on Molecular Sieve Carbon," *Chem. Eng. Sci.*, **44,** 1723 (1989).

Kayser, J. C., and K. S. Knaebel, "Pressure Swing Adsorption: Development of an Equilibrium Theory for Binary Gas Mixtures with Nonlinear Isotherms," *Chem. Eng. Sci.*, **44,** 1 (1989).

Knaebel, K. S., and F. B. Hill, "Pressure Swing Adsorption: Development of Equilibrium Theory of Gas Separations," *Chem. Eng. Sci.*, **40,** 2351 (1985).

Mitchell, J. E., and L. H. Shendalman, " Study of Heatless Adsorption in the Model System CO_2 in He: II," *AIChE Symp. Ser.*, No. 134, 25 (1973).

Nakao, S., and M. Suzuki, "Mass Transfer Coefficient in Cyclic Adsorption and Desorption," *J. Chem. Eng. Japan,* **16,** 114 (1983).

Raghavan, N.S., and D. M. Ruthven, "Pressure Swing Adsorption: III. Numerical Simulation of a Kinetically Controlled Bulk Gas Separation," *AIChE J.*, **31,** 2017 (1985).

Raghavan, N.S., M. M. Hassan, and D. M. Ruthven, "Numerical Simulation of a PSA System Using a Pore Diffusion Model," *Chem. Eng. Sci.*, **41,** 2787 (1986).

Ruthven, D. M., N. S. Raghavan, and M. M. Hassan, "Adsorption and Diffusion of Nitrogen and Oxygen in a Carbon Molecular Sieve," *Chem. Eng. Sci.*, **41,** 1325 (1986).

Shendalman, L. H., and J. E. Mitchell, "A Study of Heatless Adsorption in the Model System CO_2 in He: I," *Chem. Eng. Sci.*, **27,** 1449 (1972).

Shin, H.-S., and K. S. Knaebel, "A Theoretical Study of Diffusion-Induced Separation," *AIChE J.*, **33,** 654 (1987).

Turnock, P. H., and R. H. Kadlec, "Separation of N_2 and CH_4 via Periodic Adsorption," *AIChE J.*, **17,** 335 (1971).

Yang, R. T., *Gas Separation by Adsorption Processes,* Butterworths, Boston, MA (1987).

Manuscript received Jan. 3, 1989, and revision received June 5, 1990.